


# Resonance Raman spectroscopic analysis of the iron–sulfur cluster redox chain of the *Ralstonia eutropha* membrane-bound [NiFe]-hydrogenase

Elisabeth Siebert<sup>1</sup> | Andrea Schmidt<sup>2</sup> | Stefan Frielingsdorf<sup>1</sup> |  
Jacqueline Kalms<sup>2,3</sup> | Uwe Kuhlmann<sup>1</sup> | Oliver Lenz<sup>1</sup> | Patrick Scheerer<sup>2</sup> |  
Ingo Zebger<sup>1</sup> | Peter Hildebrandt<sup>1</sup> 

<sup>1</sup>Institute of Chemistry, Technical University of Berlin, Berlin, Germany

<sup>2</sup>Institute of Medical Physics and Biophysics (CC2), Charité—University Medicine Berlin, Free University of Berlin, Humboldt University of Berlin, Berlin, Germany

<sup>3</sup>Leicester Institute of Structural and Chemical Biology, University of Leicester, Leicester, UK

## Correspondence

Patrick Scheerer, Charité—  
Universitätsmedizin Berlin, Freie  
Universität Berlin, Humboldt-Universität  
zu Berlin, Institute of Medical Physics and  
Biophysics (CC2), Charitéplatz 1, D-10117  
Berlin, Germany.  
Email: patrick.scheerer@charite.de

Ingo Zebger and Peter Hildebrandt,  
Institut für Chemie, Technische  
Universität Berlin, Sekr. PC14, Straße des  
17. Juni 135, D-10623 Berlin, Germany.  
Email: ingo.zebger@tu-berlin.de;  
hildebrandt@chem.tu-berlin.de

## Funding information

European Union; European Union, Grant/  
Award Number: 810856; Einstein  
Foundation Berlin; *Deutsche  
Forschungsgemeinschaft*; European  
Synchrotron Radiation Facility; Helmholtz  
Zentrum Berlin für Materialien und  
Energie

## Abstract

Iron–sulfur (Fe–S) centers are versatile building blocks in biological electron transfer chains because their redox potentials may cover a wide potential range depending on the type of the cluster and the specific protein environment. Resonance Raman (RR) spectroscopy is widely used to analyze structural properties of such cofactors, but it remains still a challenge to disentangle the overlapping signals of metalloproteins carrying several Fe–S centers. In this work, we combined RR spectroscopy with protein engineering and X-ray crystallography to address this issue on the basis of the oxygen-tolerant membrane-bound hydrogenase from *Ralstonia eutropha* that catalyzes the reversible conversion of hydrogen into protons and electrons. Besides the NiFe-active site, this enzyme harbors three different Fe–S clusters constituting an electron relay with a distal [4Fe–4S], a medial [3Fe–4S], and an unusual proximal [4Fe–3S] cluster that may carry a hydroxyl ligand in the superoxidized state. RR spectra were measured from protein crystals by varying the crystal orientation with respect to the electric field vector of the incident laser to achieve a preferential RR enhancement for individual Fe–S clusters. In addition to spectral discrimination by selective reduction of the proximal cluster, protein engineering allowed for transforming the proximal and medial cluster into standard cubane-type [4Fe–4S] centers in the C19G/C120G and P242C variants, respectively. The latter variant was structurally characterized for the first time in this work. Altogether, the entirety of the RR data

Elisabeth Siebert and Andrea Schmidt contributed equally to this work.

This is an open access article under the terms of the Creative Commons Attribution License, which permits use, distribution and reproduction in any medium, provided the original work is properly cited.

© 2021 The Authors. *Journal of Raman Spectroscopy* published by John Wiley & Sons Ltd.

provided the basis for identifying the vibrational modes characteristic of the various cluster states in this “model” enzyme as a prerequisite for future studies of complex (FeS)-based electron transfer chains.

#### KEYWORDS

electron transfer, hydrogenase, iron–sulfur cluster, protein crystals, Raman spectroscopy

## 1 | INTRODUCTION

Electron transfer chains in enzymes typically utilize an array of cofactors that are spatially arranged in the protein structure to ensure an efficient electron transport over long distances. In many cases, the electron relay is based on iron–sulfur (Fe–S) centers, including two, three or four Fe ions coordinated by cysteine residues and inorganic sulfur atoms.<sup>[1–5]</sup> The redox potentials of these cofactors are controlled by the type of the Fe–S cluster and its specific interaction with the protein environment and can span a wide potential range from  $-700$  to  $+450$  mV (vs. NHE).<sup>[6]</sup> Thus, Fe–S clusters are versatile cofactors adapted for fast electron transfer between protein sites of quite different potential levels.

To elucidate electron transfer processes along Fe–S chains, the choice of methods is rather restricted. Unlike other types of redox cofactors, UV–vis absorption spectroscopy, which is typically used for redox titrations, is blind towards most reduced Fe–S clusters and can hardly distinguish between the different cluster types.<sup>[7]</sup> Electron paramagnetic resonance (EPR) spectroscopy is restricted to non-zero spin states and thus yields only an incomplete picture about Fe–S clusters.<sup>[8]</sup> Mößbauer spectroscopy is able to probe different spin and redox states of Fe–S clusters and allows distinguishing different structures.<sup>[9]</sup> However, application of this technique requires  $^{57}\text{Fe}$  labeling. Also resonance Raman (RR) spectroscopy is associated with a drawback because resonance enhancement of the vibrational modes depends on a distinct electronic transition, limiting the detection of Fe–S clusters in the oxidized state, similar to UV–vis spectroscopy.<sup>[10]</sup> Unlike UV–vis spectroscopy, however, RR spectroscopy provides a better spectral resolution, which enables an unambiguous identification of the cluster type. In fact, the Fe–S cluster manifold has been the subject of a large number of RR spectroscopic studies revealing characteristic vibrational signatures of a large number of Fe–S centers, including [2Fe–2S], [3Fe–4S], and [4Fe–4S] clusters.<sup>[10,11]</sup> Nevertheless, it remains a formidable challenge to disentangle the RR spectra of entire electron transfer chains in terms of their individual components, even if each of them belongs to a different Fe–S cluster type.

Here, we analyzed by RR spectroscopy the electron transfer chain of the intensely studied oxygen-tolerant membrane-bound [NiFe]-hydrogenase (MBH) from *Ralstonia eutropha* (Figure 1). Our “model” enzyme catalyzes the oxidation of molecular hydrogen into protons and electrons at a Ni–Fe center, in which the two metal ions are linked via two bridging cysteines. The Ni ion is further coordinated by two cysteines whereas the Fe carries additionally two cyanide and CO ligands. Efficient oxidation of  $\text{H}_2$  requires the rapid removal of electrons from the active site, which is mediated by three different Fe–S clusters, named proximal, medial, and distal cluster according to their location relative to the catalytic center. The medial and distal clusters are prototypical [3Fe–4S] and [4Fe–4S] clusters, respectively. The proximal Fe–S cluster, by contrast, exhibits a quite unusual structure.<sup>[12–14]</sup> Here, four iron ions are coordinated by three sulfides and six cysteine-derived thiolate sulfurs, which enable the [4Fe–3S] cluster to undergo redox-dependent structural and conformational changes. In contrast to conventional Fe–S clusters, which usually switch between two different redox states, the [4Fe–3S] cluster can adopt even three redox states under physiological conditions. No structural changes occur when the cluster switches between the reduced and oxidized state. Transition from the oxidized to the superoxidized state, however, is accompanied with the exchange of the coordination of one iron (named Fe4) from a sulfide ligand to the backbone nitrogen of a cysteine residue (Cys20). A second cluster-bound Fe (named Fe1) becomes coordinated by a hydroxyl ligand in the superoxidized form of the [4Fe–3S] cluster.<sup>[12]</sup> This unique structural change has been attributed to the cluster’s capability to switch between three redox states at physiological potentials and the corresponding  $\text{O}_2$  tolerance of the MBH, that is, its unusual capacity to sustain catalysis under aerobic conditions.

In this work, we employed a combined approach of protein engineering, X-ray crystallography, and RR spectroscopy to determine the characteristic vibrational signatures of the three Fe–S clusters of MBH. The RR spectroscopic experiments were carried out on MBH crystals at 77 K. First, RR spectra of native MBH crystals were measured as a function of the crystal orientation with

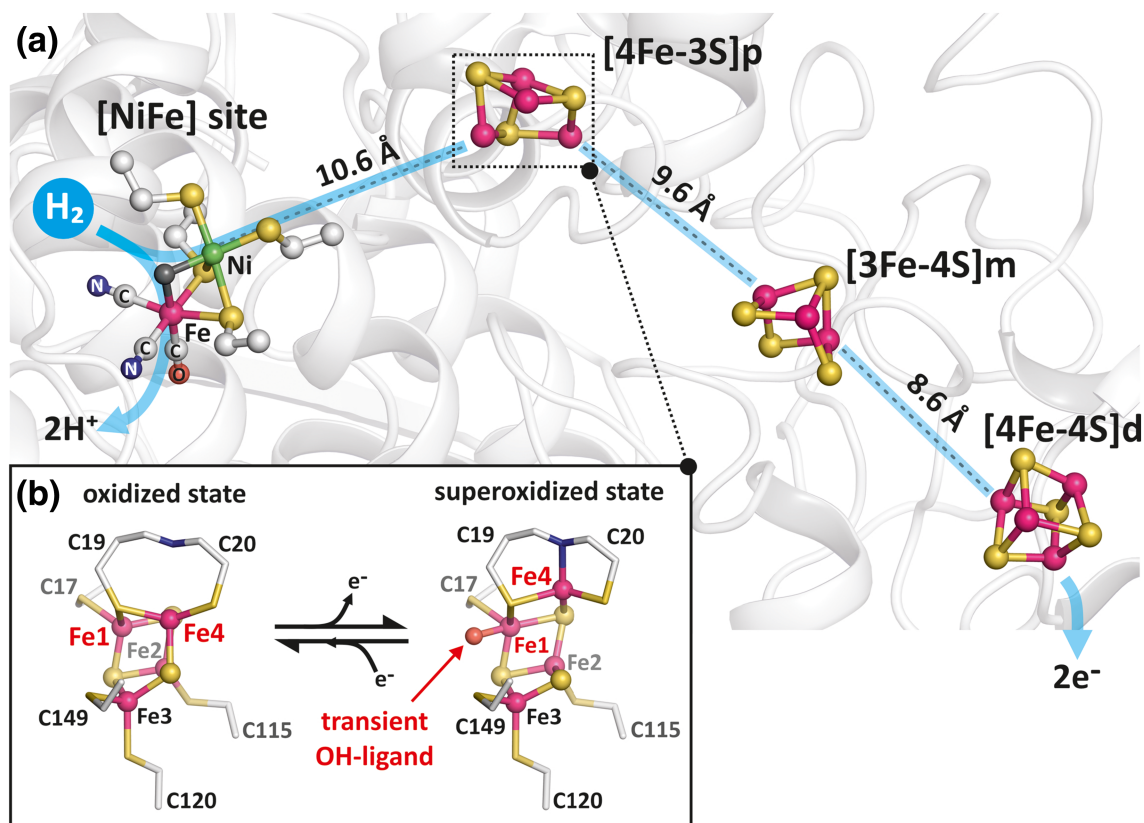


**FIGURE 1** Schematic representation of the metal cofactors in the as-isolated native membrane-bound [NiFe]-hydrogenase (MBH): (a) [NiFe] active site, proximal [4Fe-3S]p, medial [3Fe-4S]m, and distal [4Fe-4S]d clusters are represented as ball and sticks with their distances from each other as found in the crystal structure.<sup>[12]</sup> (b) Close-up of the proximal [4Fe-3S]p in two redox states as oxidized and superoxidized form. The superoxidized [4Fe-3S]p contains a transient Fe1-bound OH group<sup>[12,13]</sup>

respect to the electric field vector of the incident laser radiation. This strategy exploits the different orientations of the transition dipole moments of the three Fe-S clusters relative to the crystal axes. In this way, a preferential enhancement of RR-active modes for the individual Fe-S clusters can be achieved upon varying the angle of the electric field vector of the incident laser light with respect to the principal crystal long [*c*] axis of the needle-shaped crystals. Second, additional spectroscopic information was obtained by selective reduction of the proximal [4Fe-3S] cluster. Third, further spectral discrimination was achieved by a comparative analysis of native MBH with MBH variants in which cluster-coordinating or adjacent residues were exchanged. This included the previously investigated C19G/C120G variant<sup>[15]</sup> and the P242C variant that was characterized for the first time in this work. These exchanges revealed a four-cysteine coordination as prototypical [4Fe-4S] cluster of both the proximal and the medial Fe-S clusters.

## 2 | MATERIALS AND METHODS

### 2.1 | Protein expression and crystallization

Purification and crystallization of the heterodimeric MBH from *R. eutropha* H16 was described previously.<sup>[16]</sup> The P242C variant of MBH was crystallized under aerobic and anaerobic conditions and the structures were analyzed as described in detail in the supporting information (section 1, Table S2). The crystals of all MBH variants studied in this work belong to the orthorhombic space group *P*<sub>2</sub><sub>1</sub><sub>2</sub><sub>1</sub><sub>2</sub><sub>1</sub>.<sup>[14]</sup>

### 2.2 | RR spectroscopy

RR spectra were measured using a confocal Raman spectrometer (LabRam HR-800, Jobin Yvon) coupled to a

liquid nitrogen-cooled charge-coupled device (CCD). The spectral resolution was limited by the wavenumber increments per pixel of the CCD camera, corresponding to approximately  $1.0\text{ cm}^{-1}$  for the excitation wavelength of 457 nm provided by an Ar ion laser (coherent). The laser beam was focused on the sample surface by a Nikon 20 $\times$  objective with a working distance of 20.5 mm and a numeric aperture of 0.35, yielding a spot size of approximately 4  $\mu\text{m}$  in diameter. The laser power at the sample was set to 1 to 2 mW, and the temperature was kept at 77 K, using a Linkam THMS600 freezing microscope stage. Accumulation times were 120–300 s with up to 30 repetitions.

All RR spectra were obtained from single MBH crystals. In the standard configuration ( $\theta = 0^\circ$ ), the long axis of the needle-shaped MBH crystals, referring to the *c*-axis of the crystals unit cell, was always aligned parallel to the electric field vector  $\vec{E}$  of the linearly polarized incident laser beam (see Figure S7). To vary  $\theta$ , a half-wave plate in the excitation pathway of the setup was used to rotate the

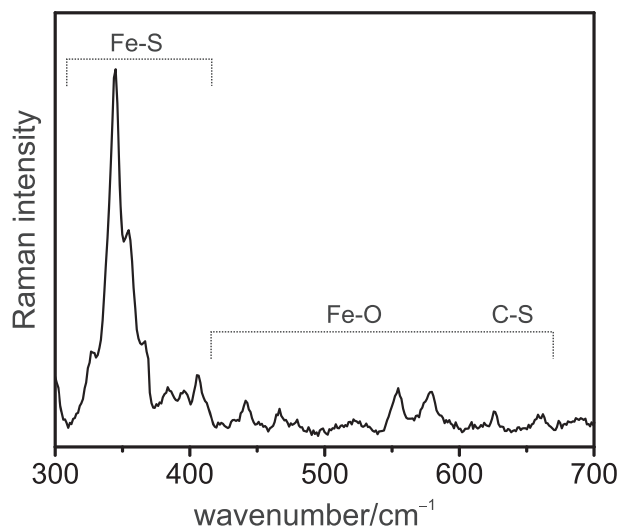


**FIGURE 2** Resonance Raman (RR) spectrum of a single crystal of superoxidized membrane-bound [NiFe]-hydrogenase (MBH), showing the regions of the Fe–S stretching and Fe–OH/C–S modes. The spectrum was obtained with 457-nm excitation at 77 K

electric field vector. This ensured that for each  $\theta$ , the same spot on the sample surface was probed. The polarization-dependent sensitivity of the spectrometer was compensated by a quarter wave plate placed in front of the entrance slit. All spectra were calibrated against the  $274.0\text{-cm}^{-1}$  peak of ice present on the protein crystals.

### 3 | RESULTS AND DISCUSSION

#### 3.1 | Strategy for identifying RR marker bands of the various Fe–S clusters

Previously, wavelength-dependent studies on MBH crystals and solutions revealed that by use of a 457 nm excitation the corresponding RR spectra of MBH may include contributions of all Fe–S centers and the [NiFe] active site in a redox-dependent manner (Figures 1, 2, and S4).<sup>[17]</sup> Definition and nomenclature of the various redox states are given in the Supporting Information (Table S1). In the  $\text{H}_2$ -reduced enzyme, the resonance enhancement of the Fe–S stretching modes is very weak such that the contribution of the Fe–S clusters to the RR spectra can be neglected. Instead, the  $\text{Ni}_a\text{-L}$  state of the active site gives rise to distinct RR bands in the region between 400 and  $700\text{ cm}^{-1}$ .<sup>[17,18]</sup> By contrast, in the as-isolated, superoxidized enzyme, the active site resides predominately in the  $\text{Ni}_r\text{-B}$  state, which is characterized by a hydroxy group bridging the nickel and iron and minor amounts of the one electron reduced  $\text{Ni}_r\text{-S}$  state. Active site-related RR bands of the potential photoproduct of the latter, lacking the bridging ligand, the so called  $\text{Ni}_a\text{-S}$  state, are hardly detectable.<sup>[18]</sup> Therefore, this spectral region is dominated by the Fe–OH modes of the superoxidized proximal cluster (Figure 2).<sup>[12,18]</sup> The proximal cluster in both superoxidized states, with and without the Fe-bound hydroxy ligand, as well as the oxidized medial and distal clusters give rise to relatively strong RR bands between 300 and  $400\text{ cm}^{-1}$  (Figure 2). Thus, the spectrum may include contributions from up to four oxidized Fe–S cluster states (Table 1). To identify the main Fe–S modes of

Variant/redox state	Proximal	Medial	Distal
MBH <sup>native</sup> /superoxidized	OH-occupied [4Fe–3S]	[3Fe–4S]	[4Fe–4S]
MBH <sup>native</sup> /superoxidized	OH-free [4Fe–3S]	[3Fe–4S]	[4Fe–4S]
MBH <sup>native</sup> /ascorbate-reduced	[4Fe–3S] <sup>a</sup>	[3Fe–4S]	[4Fe–4S]
MBH <sup>P242C</sup> , superoxidized	OH-occupied [4Fe–3S]	[4Fe–4S]	[4Fe–4S]
MBH <sup>C19G/C120G</sup> , oxidized	[4Fe–4S]	[3Fe–4S]	[4Fe–4S]

**TABLE 1** Fe–S cluster types present at the proximal, medial and distal positions of the electron transfer chains in MBH proteins used for RR spectroscopic analysis

Abbreviations: MBH, membrane-bound [NiFe]-hydrogenase; RR, Resonance Raman.

<sup>a</sup>(partially) Reduced state; not detectable in the RR spectrum.

the individual Fe–S cluster states, we employed different approaches to simplify the spectra via spectral discrimination. These were (i) orientation-dependent RR measurements of MBH crystals to achieve a preferential enhancement of the Raman bands of individual clusters, (ii) selective (partial) reduction of the proximal cluster by ascorbate, and (iii) conversion of the proximal [4Fe–3S] and medial [3Fe–4S] clusters into [4Fe–4S] cluster species by site-directed amino acid exchanges (Table 1).

### 3.2 | Orientation-dependent RR spectroscopy of MBH crystals

As shown in earlier studies, the most prominent RR bands of the [4Fe–4S] and [3Fe–4S] clusters were observed at approximately 337 and 348  $\text{cm}^{-1}$ , respectively, which are attributed to the same type of mode ( $\nu_b$ ).<sup>[19,20]</sup> It originates from the Fe–S stretchings including bridging sulfur atoms. The excitation profile and the low depolarization ratio of the mode point to a totally symmetric character with reference to an ideal cube-derived symmetry. Its intensity is mainly provided via an A-term enhancement mechanism in resonance with the electronic charge-transfer transition. Correspondingly, one would expect that the intensity scales with  $(\cos\beta)^2$ , where  $\beta$  is the angle defined by the vectors of the electric field  $\vec{E}$  and the transition dipole moment  $\vec{\mu}$ .<sup>[21]</sup> Given that the individual transition dipole moments of the three Fe–S clusters adopt different orientations in the protein, there will be a specific angle  $\beta$ , which ensures a selective enhancement of the modes of one cluster compared with those of the other two clusters. To exploit this principle for an efficient spectral discrimination in orientation-dependent RR spectroscopy of single protein crystals, an identical orientation of all molecules in the unit cell is required. However, MBH crystallizes in the orthorhombic space group  $P2_12_12_1$ , including four asymmetric units, each of them harboring one MBH heterodimer.<sup>[14]</sup> Thus, the projection of  $\vec{\mu}$  of a given Fe–S center on the  $c$ -axis of the crystal and, thus, on  $\vec{E}$  is different for each hydrogenase molecule in the unit cell. Consequently, the angle dependence of the cluster-specific enhancement of  $\nu_b$  is somewhat blurred. This is also true for the second main band located between 360 and 368  $\text{cm}^{-1}$ , which is related to Fe–S stretchings involving the terminal cysteine sulfur atoms ( $\nu_t$ ).<sup>[10,20]</sup> Because this mode is most likely enhanced via vibronic coupling (B-term scattering), the intrinsic enhancement does not follow a simple  $(\cos\beta)^2$  dependence. As a consequence, the angle-dependent RR spectra of MBH single crystals are expected to include varying contributions of the individual clusters but do not display a complete spectral separation.

For the orientation-dependent experiments, aerobically grown MBH crystals were used. Among the various crystals prepared in this way, the ratio between the superoxidized state with and without hydroxyl ligand varied substantially.<sup>[12]</sup> For the present angle-dependent measurements, we therefore selected crystals with the highest possible OH ligand population of the [4Fe–3S] cluster as determined by the characteristic Fe–OH modes between 500 and 600  $\text{cm}^{-1}$  (vide infra).<sup>[12,17]</sup> The orientation-dependent spectra were obtained from such a single MBH crystal, with increments of typically 20° in the range from  $\theta = 0^\circ$  to 180° (Figure S5). Selected examples are shown in Figure 3. The spectra were normalized with respect to the integral intensity of the most intense bands in the region of the Fe–S stretching modes between 330 and 375  $\text{cm}^{-1}$ .

At an angle of 0°, the spectrum shows the characteristic signature of the proximal [4Fe–3S] cluster with bound hydroxyl group in the region above 400  $\text{cm}^{-1}$ , including the marker bands for the Fe–OH stretching modes at 554 and 578  $\text{cm}^{-1}$ , Fe–O torsional modes below 500  $\text{cm}^{-1}$ , and C–S stretching modes of Cys19 at 625 and 660  $\text{cm}^{-1}$  assigned in our previous work (Figure 3, right).<sup>[17]</sup> All these bands have maximum relative intensity at parallel excitation ( $\theta = 0^\circ$ ) such that the corresponding Fe–S stretching modes are attributed to band components with peak maxima at 344.5 and 354.5  $\text{cm}^{-1}$  (Figure 3, left). At excitation angles above 50°, the spectral pattern changed substantially. The intensities of the [4Fe–3S] cluster-related bands (with bound OH) at higher wavenumbers strongly decreased and became comparable with the very weak bands of the Ni<sub>a</sub>–S state of the [NiFe] active site (560 and 590  $\text{cm}^{-1}$ ),<sup>[17]</sup> which are slightly above the noise level at 90° (Figure 3, right). Hence, the spectral changes in the Fe–S stretching region (Figure 3, left) observed at 70° and 90° reflect the increased spectral contribution of the medial and distal Fe–S clusters. These changes include a broadening of the prominent band envelope at 344.5  $\text{cm}^{-1}$ . The increased intensity on its low-wavenumber tail points to a stronger enhancement of a component below 338  $\text{cm}^{-1}$  (Figure 3, left). Furthermore, the spectrum displays a significant intensity increase of the 367  $\text{cm}^{-1}$  peak at 70° and even more pronounced at 90°. This is presumably due to the enhancement of two closely spaced bands, as concluded from the non-Lorentzian band profile. For a better illustration of these changes, we have generated a difference spectrum by subtracting the spectrum measured at 90° from that at 0°. The negative peaks at approximately 336 and 362  $\text{cm}^{-1}$  are in good agreement with those reported for [4Fe–4S] centers<sup>[19]</sup> and are therefore tentatively attributed to the distal [4Fe–4S] cluster of MBH.

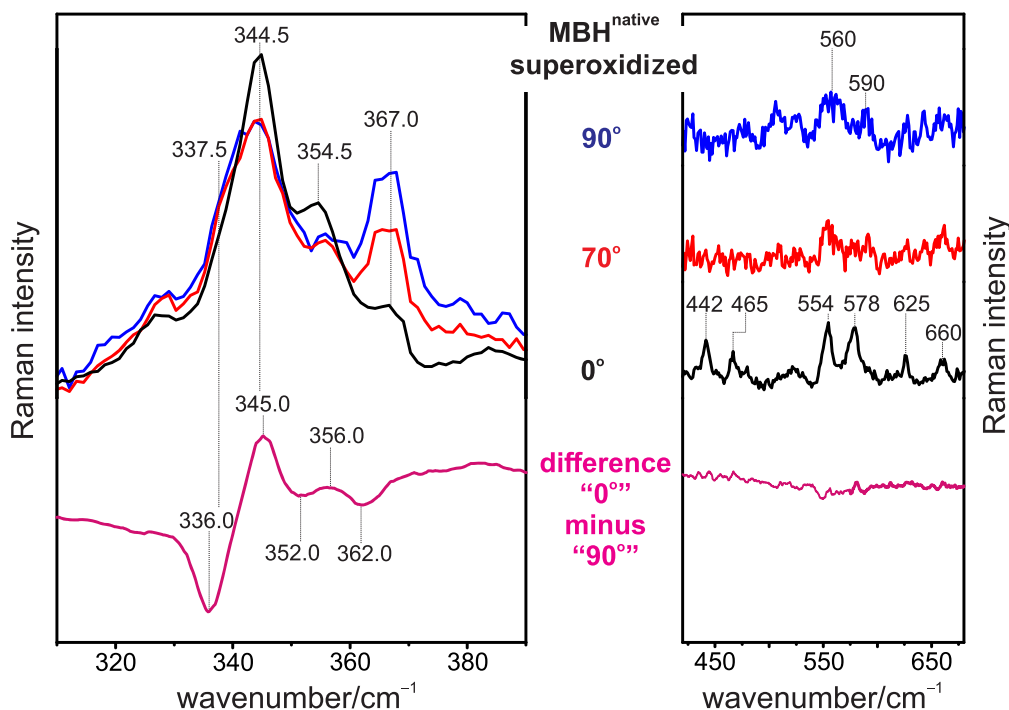


**FIGURE 3** Resonance Raman (RR) spectra of a single crystal of superoxidized membrane-bound [NiFe]-hydrogenase (MBH) with Fe1-bound OH group at different orientations of the electric field vector of the incident radiation with respect to the  $c$ -axis of the crystal. The magenta trace represents the difference spectrum (“0°” minus “90°”). The weight of the subtraction was chosen for the best possible visualization of the spectral changes. All spectra were obtained with 457-nm excitation at 77 K

### 3.3 | Analysis of MBH crystals with different hydroxyl ligand occupation of the proximal [4Fe-3S] cluster in the superoxidized state

Next, we compared the RR spectra measured at  $\theta = 0^\circ$  of the MBH crystals in the superoxidized state with high OH<sup>-</sup> occupation of the [4Fe-3S] cluster (described above) with selected MBH crystals lacking the OH<sup>-</sup> ligand of the [4Fe-3S] cluster (Figure 4). Presence or absence of the hydroxyl ligand was verified by inspection of the spectral region between 420 and 680 cm<sup>-1</sup> (Figure 4, right). The position of the  $\nu_b$  Fe-S stretching mode remained unchanged (344.5 cm<sup>-1</sup>) in the spectrum of the MBH crystal lacking the OH<sup>-</sup> ligand of the [4Fe-3S] cluster. However, the intensity at 367.5 cm<sup>-1</sup> increased at the expense of the 356.0 cm<sup>-1</sup> band, which is prominent in the crystal with high OH<sup>-</sup> occupation of the [4Fe-3S] cluster. The spectral changes become even more prominent in the corresponding difference spectra. The data allow to attribute the 367.5 cm<sup>-1</sup> band to the  $\nu_t$  mode of the OH<sup>-</sup>-free [4Fe-3S] cluster and to confirm the assignment of the 356.0 cm<sup>-1</sup> band to the [4Fe-3S] cluster

species carrying the OH<sup>-</sup> ligand. As there is no negative peak visible the 344.5 cm<sup>-1</sup> region of the difference spectrum, the corresponding  $\nu_b$  mode seems to be independent of OH<sup>-</sup> binding at the proximal cluster. These assignments were confirmed by the comparison with MBH treated by ascorbate, which exclusively reduced the proximal cluster partially to its oxidized state,<sup>[15]</sup> recognizable by the shift of the bridging Fe-S  $\nu_b$  mode to lower wavenumbers in both cases (Figure S6).

### 3.4 | Structural analysis of the P242C variant of MBH

To unravel the spectral contributions of the medial and distal clusters of MBH (Figure 3, left), we decided to convert the medial [3Fe-4S] cluster into a [4Fe-4S] species by replacing Pro242 of the MBH small subunit by a cysteine (Figure 5). Similar cluster transformations in the oxygen-sensitive [NiFe]-hydrogenase from *Desulfovibrio fructosovorans* and the O<sub>2</sub>-tolerant [NiFe]-hydrogenase Hyd-1 from *Escherichia coli* have previously been described by Rousset et al. as well as Roessler et al.,

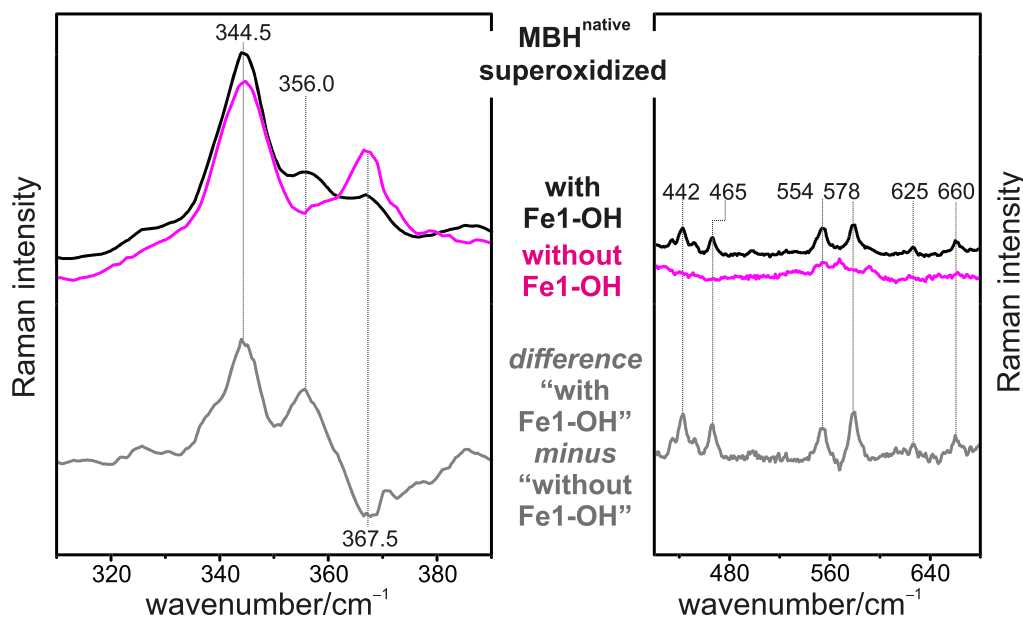


**FIGURE 4** Resonance Raman (RR) spectra of single crystals of superoxidized membrane-bound [NiFe]-hydrogenase (MBH) with (black) and without Fe1-bound OH group (magenta), obtained with 457-nm excitation at 77 K. The crystals were aligned with the *c*-axis of the crystal parallel to the electric field vector of the incident radiation. The gray trace presents the difference spectrum (“MBH with Fe1-bound OH group” minus “MBH without Fe1-bound OH group”). The weight of the subtraction was chosen for the best possible visualization of the spectral changes

respectively.<sup>[22,23]</sup> Indeed, crystal structure analysis of the MBH<sup>P242C</sup> variant, which was purified and crystallized under the same conditions as for native MBH, revealed the presence of a medial [4Fe–4S] cluster, ligated by the three conserved cysteines Cys230, Cys249, and Cys252 in addition to the artificially inserted cysteine Cys242 (Figure 5a). The structures of the distal [4Fe–4S] cluster and the [NiFe] active site remained essentially unchanged by the Pro242-to-Cys substitution. As expected, the cubic geometry of the medial cluster was not affected in crystals grown under anaerobic conditions in the presence of H<sub>2</sub>, which generally leads to the reduction of all MBH cofactors.<sup>[12,14]</sup> However, we noted several modifications at the proximal [4Fe–4S] cluster of the MBH<sup>P242C</sup> variant. In the as-isolated superoxidized enzyme, three out of six coordinating cysteines occur as S-hydroxycysteines (CSO). The corresponding hydroxyl group occupancy was approximately 60% for CSO19 and 40% for CSO20/CSO120. In addition, the Fe2-coordinating Cys115 adopts two different conformations, and Fe4 was found at two, equally occupied positions separated by 0.57 Å. A detailed description of the MBH<sup>P242C</sup> structure, including a discussion on possible functional implications of the P242C exchange, is given in the supporting information (sections 2 and 3, Figures S1–S3).

### 3.5 | RR spectroscopic analysis of MBH variants carrying engineered Fe–S clusters

Although the Pro242Cys exchange caused indeed the desired transformation of the medial [3Fe–4S] cluster into a [4Fe–4S] cluster, the same amino acid substitution also significantly perturbed the structure of the proximal [4Fe–3S] cluster in the superoxidized enzyme (vide supra). The modifications of the [4Fe–3S] cluster, however, seem to have only little effect on the RR spectra. In particular, the region of the characteristic Fe–OH bands between 420 and 680 cm<sup>−1</sup> is very similar to that of native MBH (Figure 6, left). To remove all band contributions related to the proximal cluster in the Fe–S stretching region, we therefore calculated a difference spectrum (“native” minus “P242C”), revealing positive and negative signals attributable to the medial and distal cluster, respectively (Figure 6, left). While the negative bands at 336.5 and 362.0 cm<sup>−1</sup> can be assigned to the distal [4Fe–4S] cluster, the corresponding positive signals at 345.0 and 367.0 cm<sup>−1</sup> can be attributed to the medial [3Fe–4S] cluster. This assignment relies on the assumption that the medial [4Fe–4S] cluster of the MBH<sup>P242C</sup> variant gives rise to the same RR signature as the distal [4Fe–4S] cluster of native MBH and that possible structural perturbations of the proximal cluster in the P242C

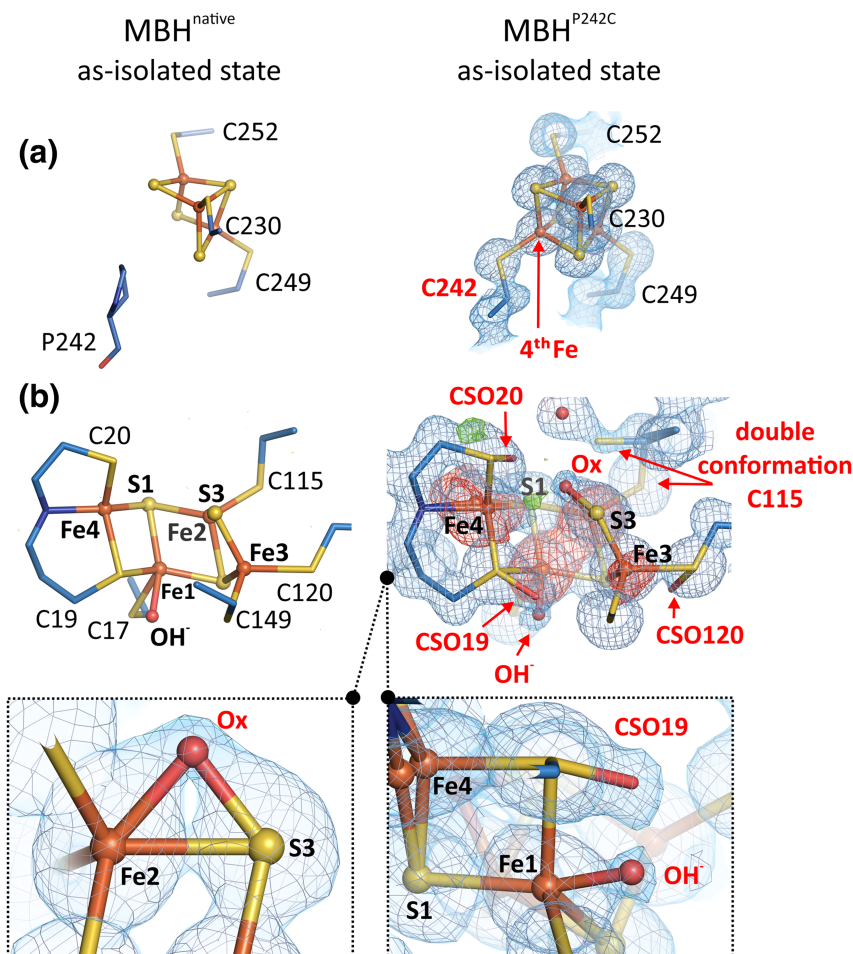


**FIGURE 5** Structural changes at the proximal and medial Fe-S clusters due to the P242C amino acid substitution in membrane-bound [NiFe]-hydrogenase (MBH). (a) *Left*: the medial [3Fe-4S] cluster of the as-isolated native MBH is shown as ball and sticks. *Right*: in the variant MBH<sup>P242C</sup>, a cubic [4Fe-4S] cluster is established in the medial position of the electron relay (*mFo-DFc* electron density map shown as blue mesh, contoured at 1  $\sigma$  level). An additional Fe ion (highlighted in red) completes the former native [3Fe-4S] cluster (left) to form a cubane [4Fe-4S] cluster. This is made possible by the ligation of a fourth Fe by the artificial Cys242 (highlighted in red). (b) *Left*: the proximal [4Fe-3S] cluster of the as-isolated native MBH is shown as ball and sticks. *Right*: in the as-isolated, superoxidized MBH<sup>P242C</sup>, cysteines 19, 20, and 120, coordinating the proximal cluster of MBH<sup>P242C</sup>, carry oxygenations (named CSO19, CSO20, and CSO120). Furthermore, Cys115 occurs in a double conformation, and additional oxygenations at Fe1 and between Fe2 and S3 were observed. In the as-isolated state, all aforementioned iron ions reveal negative peaks in the *mFo-DFc* electron density (red mesh, contoured at 3.0  $\sigma$  level), indicating sub-stoichiometric occupancy. *Left*: for comparison, the native proximal [4Fe-3S] cluster with the flexible OH<sup>-</sup> ligand bound to the Fe1.<sup>[12,13]</sup> The *mFo-DFc* (blue mesh) and *mFo-DFc* (green and red mesh) electron density maps are contoured at 1.0  $\sigma$  and 3.0  $\sigma$  level, respectively. For clarity, the close-ups of Part (b, left) show with only *mFo-DFc* electron density maps in two different views. In all figures, the Fe-S clusters are depicted as ball/sticks the additional ligands as sticks

variant have no significant effect on its RR spectroscopic signature (*vide supra*). To check these assumptions, we generated difference spectra for two further variant “combinations” by subtracting the spectrum of a MBH<sup>P242C</sup> crystal from that of the C19G/C120G double substitution variant (MBH<sup>C19G/C120G</sup>) and the ascorbate-reduced native MBH protein.

Previous EPR spectroscopic investigations revealed that the proximal, most likely cubic cluster of the MBH<sup>C19G/C120G</sup> variant, mediates only a one-electron redox transition.<sup>[15]</sup> Indeed, the crystal structure

confirmed the formation of a proximal cubic [4Fe-4S] cluster upon substituting C120 and C19 with glycine.<sup>[24]</sup> Subtracting the RR spectrum of as-isolated MBH<sup>P242C</sup> from that of the as-isolated MBH<sup>C19G/C120G</sup> variant yielded a difference spectrum with positive signals in the Fe-S stretching region referring to the [3Fe-4S] cluster as well as negative bands in the Fe-OH region corresponding to the hydroxyl-ligated [4Fe-3S] cluster (Figure 7). Similarly, we compared the spectra of MBH<sup>P242C</sup> and ascorbate-reduced native MBH with RR-detectable contributions only from the medial [3Fe-4S]



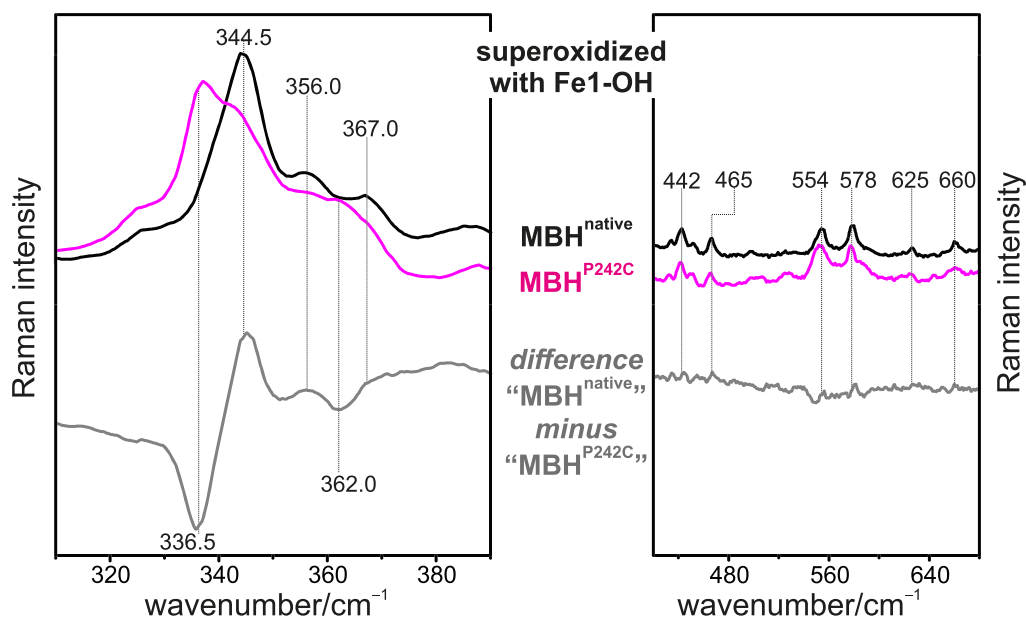


**FIGURE 6** Resonance Raman (RR) spectra of single crystals of superoxidized membrane-bound [NiFe]-hydrogenase (MBH) (black) and superoxidized MBH<sup>P242C</sup> (magenta), both with Fe1-bound OH<sup>-</sup> group, obtained with 457 nm excitation at 77 K. The crystals were aligned with the c-axis of the crystal parallel to the electric field vector of the incident radiation. The gray trace presents the difference spectrum (“MBH<sup>native</sup>,” minus “MBH<sup>P242C</sup>,”). The weight of the subtraction was chosen for the best possible visualization of the spectral changes

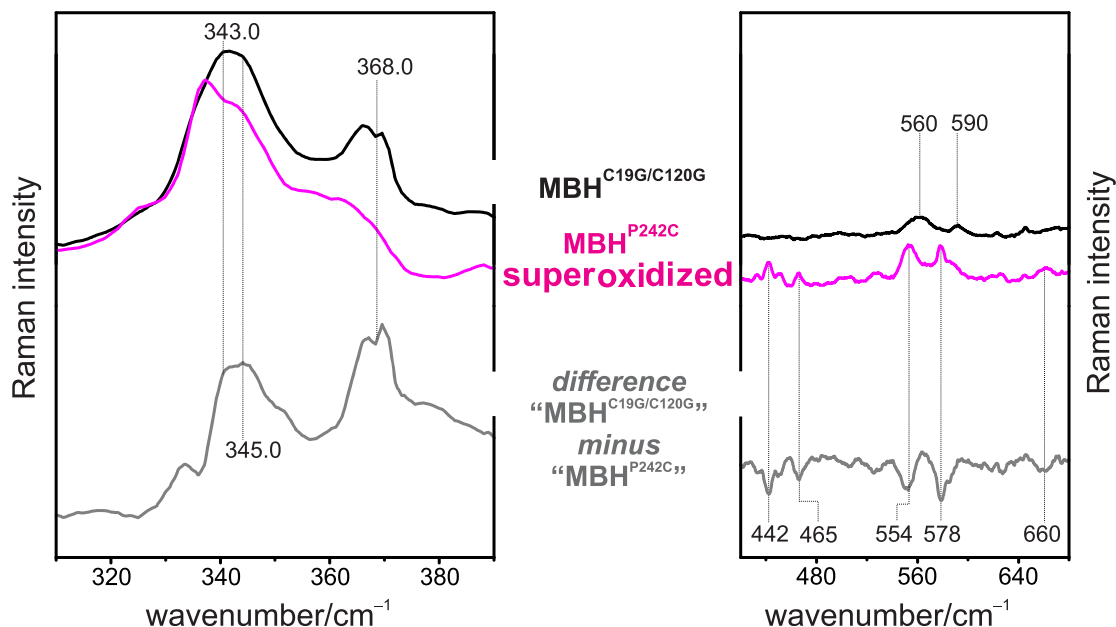


**FIGURE 7** Resonance Raman (RR) spectra of single crystals of as-isolated membrane-bound [NiFe]-hydrogenase (MBH)<sup>C19G/C120G</sup> (black) and as-isolated MBH<sup>P242C</sup> (magenta) (in the superoxidized state with Fe1-bound OH<sup>-</sup> group), obtained with 457-nm excitation at 77 K. The crystals were aligned with the c-axis of the crystal parallel to the electric field vector of the incident radiation. The gray trace presents the difference spectrum (“MBH<sup>C19G/C120G</sup>,” minus “MBH<sup>P242C</sup>,”). The weight of the subtraction was chosen for the best possible visualization of the spectral changes

and distal [4Fe–4S] cluster (Figure 8). Again, the positive peaks in the difference spectrum originate from the [3Fe–4S] cluster whereas negative signals should result from

the [4Fe–3S] cluster lacking a hydroxyl ligand and [4Fe4S]. In fact, both difference spectra display strong positive signals at 368.0 (Figure 7) and 366.5 cm<sup>-1</sup>

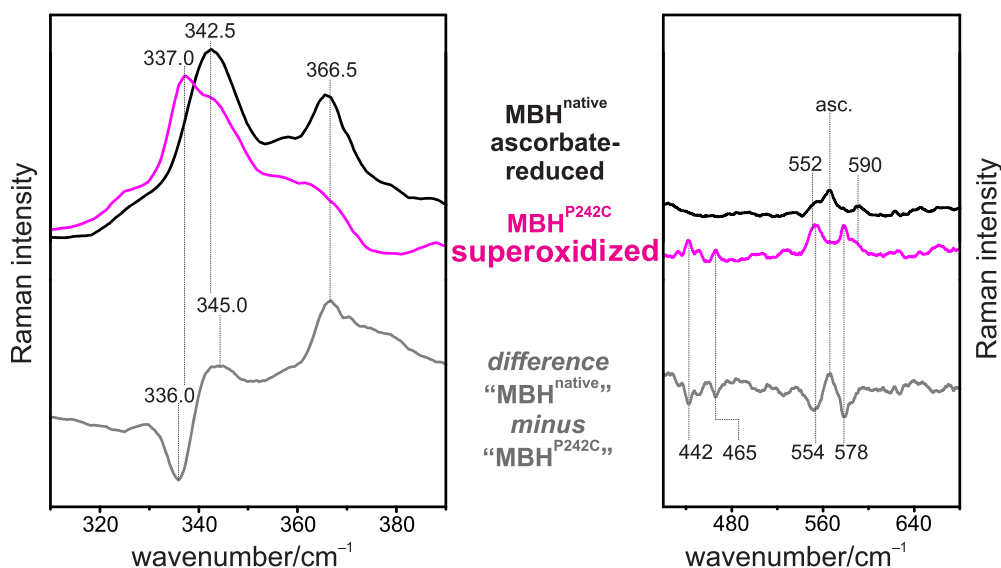


**FIGURE 8** Resonance Raman (RR) spectra of single crystals of ascorbate-reduced WT MBH (black) and superoxidized P242C with Fe1-bound OH<sup>-</sup> group (magenta), obtained with 457-nm excitation at 77 K. The crystals were aligned with the *c*-axis of the crystal parallel to the electric field vector of the incident radiation. The gray trace presents the difference spectrum (“MBH<sup>native</sup>” minus “P242C”). The weight of the subtraction was chosen for the best possible visualization of the spectral changes

(Figure 8), which compare well with the 367.0 cm<sup>-1</sup> peak in the RR spectrum of the native MBH (Figure 6). The slight variations of the peak position just reflect the limitations of the “difference” approach: (i) the structural perturbation of the proximal cluster in MBH<sup>P242C</sup> causes, unlike to the spectral region of the Fe–OH mode, deviations in the RR spectroscopic signature of the Fe–S stretching modes, and (ii) the RR spectra of the native distal [4Fe–4S] cluster are very similar but not identical to the proximal and medial [4Fe–4S] clusters generated by genetic engineering. Given these uncertainties, we conclude that the  $\nu_t$  mode of the [3Fe–4S] cluster is located at approximately 367.0 cm<sup>-1</sup>. The corresponding  $\nu_b$  mode is attributed to the positive peak at 345.0 cm<sup>-1</sup>, which is observed in all difference spectra based on the MBH<sup>P242C</sup> variant (Figures 6–8). The wavenumber of this mode is close to that of the OH-occupied [4Fe–3S] cluster (344.5 cm<sup>-1</sup>; vide supra) which accounts for the lack of a negative peak in the Fe–S stretching region of the difference spectra in Figure 7. In contrast, the  $\nu_b$  mode of the medial P242C and in turn also the distal [4Fe–4S] cluster is found to be located more distant at 336.0 cm<sup>-1</sup> (Figure 8).

The assignments of the  $\nu_b$  and  $\nu_t$  modes of all oxidized Fe–S clusters states are listed in Table 2. For the prototypical distal [4Fe–4S] and medial [3Fe–4S] clusters of MBH, the results agree very well with previously reported data obtained for other iron–sulfur proteins.<sup>[19,20]</sup> The Fe–S modes of the proximal [4Fe–3S] cluster clearly depend on

**TABLE 2** Wavenumbers of the  $\nu_b$  and  $\nu_t$  modes of the different Fe–S clusters in membrane-bound [NiFe]-hydrogenase (MBH)

Fe–S cluster	$\nu_b/\text{cm}^{-1}$	$\nu_t/\text{cm}^{-1}$
Proximal [4Fe–3S] + OH	344.5	356.0
Proximal [4Fe–3S] – OH	344.5	367.5
Medial [3Fe–4S]	345.0	368.0
Distal [4Fe–4S]	336.5	362.0

the presence of the Fe1-bound hydroxyl ligand. In the absence of the OH<sup>-</sup> ligand, the band positions are very similar to those of prototypical [3Fe–4S] clusters, whereas the presence of the hydroxyl ligand causes a substantial downshift of the Fe–S stretching mode involving the cysteine sulfur atoms.

## 4 | CONCLUSIONS

In this work, we analyzed the complex multicluster electron transfer chain of an oxygen-tolerant [NiFe]-hydrogenase, MBH from *R. eutropha*, by RR spectroscopy. The study involved three different approaches, which altogether allowed determining the characteristic Fe–S stretching modes of the superoxidized proximal [4Fe–3S] cluster with and without the Fe1-bound hydroxyl ligand as well as the oxidized medial and distal clusters. First, measuring the RR spectra of MBH crystals in different

orientations with respect to the electric field vector of the incident laser beam yielded an orientation-dependent, preferential enhancement of the modes of individual clusters. A fully selective enhancement was impaired because the crystals include four asymmetric MBH units. Second, further support for the spectral discrimination was provided by selective alteration of the proximal cluster oxidation state. Third, by site-directed mutagenesis individual clusters were modified which substantially broadened the data basis of experimental RR spectra and thus verified the vibrational assignments.

Although the individual approaches made use of the specific properties of MBH, the applicability of this procedure is not restricted to this particular enzyme. In fact, it can be adapted to other enzymes/proteins containing multiple RR-active redox centers. Once characteristic bands are identified, the experiments may be extended to (frozen) solutions of the target proteins. Thus, it may become possible to study enzymes *in operando* to determine the relative contributions of individual (oxidized) Fe–S clusters under steady-state conditions. However, due the low RR cross sections of Fe–S centers, the overall sensitivity is most likely not sufficient for true time-resolved RR studies. Such technically demanding experiments may be an option for proteins containing also cofactors other than Fe–S centers, such as hemes or flavins, which exhibit distinctly higher RR cross sections. In these cases, the present methodological concept may be even expanded by variation of the excitation wavelengths to discriminate between the different types of cofactors.

## ACKNOWLEDGEMENTS

We are grateful to Manfred Weiss and the scientific staff of the BESSY-MX/Helmholtz Zentrum Berlin für Materialien und Energie at beamlines BL14.1, BL14.2, and BL14.3 operated by the Joint Berlin MX-Laboratory at the BESSY II electron storage ring (Berlin-Adlershof, Germany) and the scientific staff of the European Synchrotron Radiation Facility (ESRF, Grenoble) at beamlines ID30A-1-3, ID30B, ID23-1, ID23-2, ID14.4, and ID29, where the data were collected, for continuous support. This work was supported by *Deutsche Forschungsgemeinschaft* (DFG, German Research Foundation) through the cluster of excellence “UniSysCat” under Germany’s Excellence Strategy-EXC2008/1-390540038 to O. L., P. S., I. Z., and P. H. as well as through the SPP 1927 “Iron sulfur for life” to I. Z. and O. L. We also thank the Einstein Center of Catalysis (EC<sup>2</sup>) funded by the Einstein Foundation Berlin for support. P. H., O. L., and I. Z. are also grateful for funding from the European Union’s Horizon 2020 research and innovation program (under grant agreement No 810856).

## ORCID

Peter Hildebrandt  <https://orcid.org/0000-0003-1030-5900>

## REFERENCES

- [1] H. Beinert, *J. Biol. Inorg. Chem.* **2000**, *5*, 2.
- [2] J. M. Hudson, K. Heffron, V. Kotlyar, Y. Sher, E. Maklashina, G. Cecchini, F. A. Armstrong, *J. Am. Chem. Soc.* **2005**, *127*, 6977.
- [3] J. Fritsch, O. Lenz, B. Friedrich, *Nat. Rev. Microbiol.* **2013**, *11*, 106.
- [4] P. Zanello, *J. Struct. Biol.* **2018**, *202*, 264.
- [5] P. Zanello, *J. Struct. Biol.* **2018**, *202*, 250.
- [6] J. Liu, S. Chakraborty, P. Hosseinzadeh, Y. Yu, S. Tian, I. Petrik, A. Bhagi, Y. Lu, *Chem. Rev.* **2014**, *114*, 4366.
- [7] F. Melin, P. Hellwig, *Chem. Rev.* **2020**, *120*, 10244.
- [8] W. R. Hagen, *J. Biol. Inorg. Chem.* **2018**, *23*, 623.
- [9] M. E. Pandelia, N. D. Lanz, S. J. Booker, C. Krebs, *Biochim. Biophys. Acta, Mol. Cell Res.* **1853**, 2015, 1395.
- [10] S. Todorovic, M. Teixeira, *J. Biol. Inorg. Chem.* **2018**, *23*, 647.
- [11] T. G. Spiro, R. S. Czernuszewicz, *Methods Enzymol.* **1995**, *246*, 416.
- [12] S. Frielingsdorf, J. Fritsch, A. Schmidt, M. Hammer, J. Löwenstein, E. Siebert, V. Pelmeshnikov, T. Jaenicke, J. Kalms, Y. Rippers, F. Lenzian, I. Zebger, C. Teutloff, M. Kaupp, R. Bittl, P. Hildebrandt, B. Friedrich, O. Lenz, P. Scheerer, *Nat. Chem. Biol.* **2014**, *10*, 378.
- [13] J. Kalms, A. Schmidt, S. Frielingsdorf, T. Utesch, G. Gotthard, D. von Stetten, P. van der Linden, A. Royant, M. A. Mroginiski, P. Carpentier, O. Lenz, P. Scheerer, *Proc. Natl. Acad. Sci. U. S. A.* **2018**, *115*, E2229.
- [14] J. Fritsch, P. Scheerer, S. Frielingsdorf, S. Kroschinsky, B. Friedrich, O. Lenz, C. M. T. Spahn, *Nature* **2011**, *479*, 249.
- [15] T. Goris, A. F. Wait, M. Saggi, J. Fritsch, N. Heidary, M. Stein, I. Zebger, F. Lenzian, B. Friedrich, O. Lenz, *Nat. Chem. Biol.* **2011**, *7*, 310.
- [16] O. Lenz, L. Lauterbach, S. Frielingsdorf, *Methods Enzymol.* **2018**, *613*, 117.
- [17] E. Siebert, Y. Rippers, S. Frielingsdorf, J. Fritsch, A. Schmidt, J. Kalms, S. Katz, O. Lenz, P. Scheerer, L. Paasche, V. Pelmeshnikov, U. Kuhlmann, M. A. Mroginiski, I. Zebger, P. Hildebrandt, *J. Phys. Chem. B* **2015**, *119*, 13785.
- [18] E. Siebert, M. Horch, Y. Rippers, J. Fritsch, S. Frielingsdorf, O. Lenz, F. Velazquez Escobar, F. Siebert, L. Paasche, U. Kuhlmann, F. Lenzian, M. A. Mroginiski, I. Zebger, P. Hildebrandt, *Angew. Chem. Int. Ed.* **2013**, *52*, 5162.
- [19] W. Fu, S. O’Handley, R. P. Cunningham, M. K. Johnson, *J. Biol. Chem.* **1992**, *267*, 16135.
- [20] M. K. Johnson, R. S. Czernuszewicz, T. G. Spiro, J. A. Fee, W. V. Sweeney, *J. Am. Chem. Soc.* **1983**, *105*, 6671.
- [21] D. A. Long, *The Raman Effect*, John Wiley and Sons, Chichester **2002**.
- [22] M. Rousset, Y. Montet, B. Guigliarelli, N. Forget, M. Asso, P. Bertrand, J. C. Fontecilla-Camps, E. C. Hatchikian, *Proc. Natl. Acad. Sci. U. S. A.* **1998**, *95*, 11625.
- [23] M. M. Roessler, R. M. Evans, R. A. Davies, J. Harmer, F. A. Armstrong, *J. Am. Chem. Soc.* **2012**, *134*, 15581.

- [24] P. Wulff, C. Thomas, F. Sargent, F. A. Armstrong, *J. Biol. Inorg. Chem.* **2016**, *21*, 121.

### SUPPORTING INFORMATION

Additional supporting information may be found online in the Supporting Information section at the end of this article.

**How to cite this article:** E. Siebert, A. Schmidt, S. Frielingsdorf, J. Kalms, U. Kuhlmann, O. Lenz, P. Scheerer, I. Zebger, P. Hildebrandt, *J Raman Spectrosc* **2021**, *52*(12), 2621. <https://doi.org/10.1002/jrs.6163>